Antiviral Research 134 (2016) 226–235

Contents lists available at ScienceDirect

Antiviral Research

journal homepage: www.elsevier.com/locate/antiviral

# Targeting flavivirus RNA dependent RNA polymerase through a pyridobenzothiazole inhibitor

Delia Tarantino [a, b, 1], Rolando Cannalire [c, 1], Eloise Mastrangelo [a, b], Romina Croci [a], Gilles Querat [d], Maria Letizia Barreca [c], Martino Bolognesi [a, b], Giuseppe Manfroni [c, **], Violetta Cecchetti [c], Mario Milani [a, b, *]

[a] Dipartimento di Bioscienze, Università di Milano, Via Celoria 26, I-20133, Milano, Italy
[b] CNR-IBF, Istituto di Biofisica, Via Celoria 26, I-20133, Milano, Italy
[c] Dipartimento di Scienze Farmaceutiche, Università degli Studi di Perugia, Perugia, Italy
[d] UMR "Emergence des Pathologies Virales" (EPV: Aix-Marseille university – IRD 190 – Inserm 1207 – EHESP), & Fondation IHU Méditerranée Infection, APHM Public Hospitals of Marseille, Marseille, France

ARTICLE INFO

*Article history:*
Received 12 July 2016
Received in revised form
12 September 2016
Accepted 16 September 2016
Available online 17 September 2016

*Keywords:*
Flavivirus
RNA dependent RNA polymerase
Crystal structure
Polymerase mutants
Non-competitive inhibition
Virus inhibition

ABSTRACT

RNA dependent RNA polymerases (RdRp) are essential enzymes for flavivirus replication. Starting from an *in silico* docking analysis we identified a pyridobenzothiazole compound, HeE1-2Tyr, able to inhibit West Nile and Dengue RdRps activity *in vitro*, which proved effective against different flaviviruses in cell culture. Crystallographic data show that HeE1-2Tyr binds between the fingers domain and the priming loop of Dengue virus RdRp (Site 1). Conversely, enzyme kinetics, binding studies and mutational analyses suggest that, during the catalytic cycle and assembly of the RdRp-RNA complex, HeE1-2Tyr might be hosted in a distinct binding site (Site 2). RdRp mutational studies, driven by *in silico* docking analysis, allowed us to locate the inhibition Site 2 in the thumb domain. Taken together, our results provide innovative concepts for optimization of a new class of anti-flavivirus compounds.



## 1. Introduction

The genus Flavivirus belongs to the *Flaviviridae* family and consists of over seventy related members, mostly transmitted by arthropods, and pathogenic to humans (Mackenzie et al., 2004). Among them, Dengue virus (DENV), West Nile virus (WNV), Japanese Encephalitis virus (JEV), Yellow fever virus (YFV), and lately Zika virus, are considered important pathogens that occupy a special area within the RNA virus world (Daep et al., 2014). Flaviviral infections are classified by the World Health Organization (WHO) as neglected tropical diseases (NTDs); nevertheless, a well-established body of environmental, demographic, and ecological evidences suggest that known and/or novel flavivirus are likely to spread to other regions of the word in the near future (http://www.who.int/csr/don/21-october-2015-zika/en/).

Flaviviruses are small, enveloped, RNA viruses whose genome consists of a 11 kb 5'-capped (+)*ss*-RNA that encodes for a single polyprotein, which is processed to yield three structural and seven non-structural (NS) proteins. The expression of NS proteins induces modifications on the host endoplasmic reticulum where viral replication takes place (Welsch et al., 2009). NS5 is a multi-domain protein endowed with N-terminal methyltransferase activity and C-terminal RNA-dependent RNA polymerase (RdRp) activity. RdRp replicates (+)RNA into (-)RNA that is later used as a template to produce large excess of the viral genome. It has been shown that NS5 initiates RNA synthesis *de novo* (*i.e.* primer-independent) using a conserved loop (the priming loop) that protrudes from the RdRp

*Abbreviations:* RdRp, RNA dependent RNA polymerase; **HeE1-2Tyr**, N-{[8-(Cyclohexyloxy)-1-oxo-2-phenyl-1H-pyrido[2,1-b][1,3]benzothiazol-4-yl] carbonyl}-L-tyrosinate; DENV, Dengue virus; WNV, West Nile virus; JEV, Japanese encephalitis virus; YFV, yellow fever virus; HCV, hepatitis C virus.

* Corresponding author. CNR, Istituto di Biofisica, Via Celoria 26, I-20133, Milano, Italy.
** Corresponding author. Department of Pharmaceutical Sciences, Università degli Studi di Perugia, Via A. Fabretti, 48, 06123, Perugia, Italy.
*E-mail addresses:* giuseppe.manfroni@unipg.it (G. Manfroni), mario.milani@unimi.it (M. Milani).

[1] These authors have contributed equally to the studies presented.

http://dx.doi.org/10.1016/j.antiviral.2016.09.007

thumb domain toward the fingers domain to assist formation of the initiation complex (Selisko et al., 2012).

An effective and specific therapy against flaviviruses is currently not available; even the broad-spectrum antiviral compound ribavirin appears ineffective for treating flavivirus infections (Leyssen et al., 2000; Malinoski et al., 1990). In the search for new antivirals, a promising strategy is to target the viral polymerase, as shown by the results obtained *versus* HIV reverse transcriptase, and with the HCV NS5B inhibitors, currently in clinical use. Although a number of DENV (and to less extent of WNV) NS5 RdRp inhibitors have been reported, to date none of these passed efficacy/safety tests in animals or in clinical trials (Lim et al., 2015; Xu et al., 2015).

In the context of a drug discovery program targeting flavivirus RdRp, we firstly analyzed *in silico* a focused library consisting of 203 published (Manfroni et al., 2014a,b; Barreca et al., 2013; Manfroni et al., 2012) and unpublished compounds, designed to target specifically HCV NS5B RdRp. The results of such *in silico* screening vs. DENV RdRp brought us to the biochemical and crystallographic characterization of one selected compound, **HeE1-2Ty**, that proved to be a micromolar inhibitor of flavivirus RdRp. Importantly, this pyridobenzothiazole-based compound, showed specific antiviral activity (in the micromolar range) in cell cultures against a panel of different flaviviruses. Here we report the chemical synthesis of **HeE1-2Tyr**, together with the crystal structure of the DENV (serotype 3, DENV3) RdRp/**HeE1-2Tyr** complex, and describe its biochemical characterization as a DENV3 RdRp inhibitor. To exert its RdRp inhibitory activity, **HeE1-2Tyr** exploits an inhibition and binding mechanism, new to RdRp, which might be extended to the design of a new class of inhibitory compounds.

## 2. Materials and methods

### 2.1. Preparation of N-{[8-(Cyclohexyloxy)-1-oxo-2-phenyl-1H-pyrido[2,1-b][1,3]benzothiazol-4-yl]carbonyl}-L-tyrosinate (HeE1-2Tyr)

For general methods: see Supplementary material.

A solution of methyl ester **6** (150 mg, 0.3 mmol) and aq 1N LiOH (0.9 mmol) in 1,4-dioxane (5 mL) was stirred for 0.5 h at room temperature. The mixture was poured into ice/water, acidified with 2N HCl (pH = 3) and extracted three times with EtOAc. The combined organic layers were washed two times with brine, dried, and evaporate under vacuum to give a crude solid which was purified by flash column chromatography eluting with $CHCl_3$/MeOH (90:10) affording the title compound **HeE1-2Tyr** (87 mg, 50%) as yellow solid: mp 260–262 °C; TLC ($CHCl_3$/MeOH, 80:20 v/v): $R_f$ = 0.40; $[\alpha]_D$ = −0.36 (0.5% p/v, MeOH); $^1$H NMR (400 MHz, DMSO-$d_6$): $\delta$ 12.80 (brs, 1H, Tyr-$CO_2$H), 9.20 (brs, 1H, Tyr-OH), 8.90–8.80 (m, 2H, Tyr-NH and H-9), 8.50 (s, 1H, H-3), 7.90 (d, $J$ = 8.7 Hz, 1H, H-6), 7.80–7.75 (m, 2H, Ar-H), 7.50–7.45 (m, 2H, Ar-H), 7.40–7.35 (m, 1H, Ar-H), 7.20 (dd, $J$ = 2.2 and 8.7 Hz, 1H, H-7), 7.15–7.10 (m, 2H, Tyr Ar-H), 6.65–6.60 (m, 2H, Tyr Ar-H), 4.70–4.60 (m, 1H, Tyr-CH), 4.45–4.35 (m, 1H, Cy-CH), 3.10 (dd, $J$ = 4.7 and 13.9 Hz, 1H, Tyr-C$H_A$H$_B$), 2.90 (dd, $J$ = 10.5 and 13.9 Hz, 1H, Tyr-CH$_A$H$_B$), 2.00–1.85 and 1.75–1.60 (each m, 2H, Cy-$CH_2$), 1.55–1.20 (m, 6H, Cy-$CH_2$); $^{13}$C NMR (100 MHz, DMSO-$d_6$): δ 173.81, 164.49, 161.32, 156.31, 156.29, 151.89, 138.98, 136.77, 133.92, 130.41, 129.36, 128.47, 127.83, 127.89, 123.13, 122.39, 120.90, 116.50, 115.45, 107.52, 105.37, 75.66, 55.13, 36.09, 31.57, 25.52, 23.48; HRMS ($m/z$): $[M]^+$ calcd. for $C_{33}H_{30}N_2O_6S$, 583.1902; found 583.1908; LC-MS: ret. time 7.35 min. Chiral HPLC: ret time$_{Zwix-(+)}$ 5.16 min; ret time$_{Zwix-(-)}$ 12.12 min, ee: 100%.

### 2.2. In silico docking

The AutoDock 4.2 software package (Morris et al., 2009) was used for a docking search on a library with 203 compounds developed as potential HCV RdRp inhibitors (Manfroni et al., 2014a,b; Barreca et al., 2013; Manfroni et al., 2012). Briefly, the atomic coordinates of the DENV3 RdRp (pdb-id: **2J7U**; (Yap et al., 2007)) were chosen as a rigid protein model, removing all water molecules. The protein was prepared using the program Python Molecule Viewer 1.4.5 (http://mgltools.scripps.edu/packages/pmv), adding hydrogen atoms and Kollman charges.

#### 2.2.1. In silico docking around the protein active site

The RdRp protein model was employed to build a discrete grid within a box of 22.1 × 29.6 × 22.1 Å$^3$, centered near the side chain of Trp795 (Autogrid 4.2; grid step size: 0.375 Å) as the explored volume for the docking search. All the compound formulas from the focused library (2D sdf format) were processed with MolConvert (ChemAxon Ltd) to generate 3D sdf format; the program Open Babel (O'Boyle et al., 2011) then converted all sdf into pdb files. After the addition of Gasteiger charges, and of the rotational constraints on every molecule in the library (MGLTools package: http://mgtools.scripps.edu/), a 'docking parameter file' was generated for each compound, to perform 30 independent genetic algorithm runs in the docking procedure. The results were analyzed with Python Molecule Viewer 1.4.5. The best two molecules (ΔG values −10.05 and −9.52 kcal/mol), were selected to be tested in *in vitro* activity assays.

#### 2.2.2. In silico docking around the thumb domain

For the purpose of a second docking analysis (see below), the priming loop of the protein (from His786 to Asp808) was removed from the pdb, leaving an open gap in the polypeptide chain. The protein was then prepared using the program Python Molecule Viewer 1.4.5 as described before. The protein model was employed to build a discrete grid within a box of 22.9 × 22.9 × 22.9 Å$^3$ dimensions, centered near the thumb domain residue Ala757. A search for the best docking sites of **HeE1-2Tyr** was performed using AutoDock 4.2 (60 genetic algorithm runs).

### 2.3. Cloning, expression and purification of the DENV3 RdRp domain

DENV3 RdRp (amino acids 272-900) was cloned into pET15b with a His6-tag at the N-ter, and expressed in *E. coli* BL21pLys cells (Noble et al., 2013). Cells were grown at 37 °C to an $OD_{600}$ 0.8, induced with 0.4 mM isopropyl β-D-thiogalactopyranoside (IPTG) and further incubated O/N at 15 °C. Cells were harvested by centrifugation and the pellet was resuspended in 20 mM Na HEPES at pH 7.0, 300 mM NaCl, 5 mM imidazole, DNase I (2 μg/ml), 20 mM $MgSO_4$ and EDTA-free complete protease inhibitors (Roche), and lysed using a cell disruptor (Basic Z Bench top 0.75 KW; Constant System). The lysate was clarified by centrifugation at 18,000 rpm for 1 h at 4 °C. The supernatant was purified through a 5 ml bed volume HiTrap nickel immobilized metal ion affinity chromatography column (G.E. Healthcare) connected to a FPLC system (G.E. Healthcare), after washing unbound protein with buffer A (20 mM Na HEPES at pH 7.0, 300 mM NaCl, EDTA-free complete protease inhibitors (Roche)) with 60 mM imidazole; RdRp was then eluted with buffer A + 255 mM imidazole. To remove the N-terminal His6-tag, 500 U of thrombin (Sigma) was added to the pooled fraction containing the RdRp, and the mixture was dialyzed O/N at 4 °C against 1 l of buffer A supplemented with 5 mM TCEP. DENV3 RdRp was further purified by size exclusion chromatography (Superdex 200) using the same buffer. The purity of the resulting RdRp was

tested through SDS-PAGE analysis. The protein was concentrated to 8 mg/ml using a 10-kDa molecular mass cut-off centrifugal concentrator (Millipore), divided into aliquots and stored at −20 °C. For expression and purification of WNV RdRp see Supplementary material.

### 2.4. DENV3 and WNV RdRp inhibition assay

RdRp activity was assessed *in vitro* following the synthesis of double-stranded RNA from a single-stranded RNA poly(C) template (Sigma-Aldrich P4903) (1 μg final quantity) and 100 μM GTP, in a reaction mixture containing 20 mM Tris/HCl (pH 7.5), 1 mM DTT, 25 mM NaCl, 5 mM $MgCl_2$, 0.3 mM $MnCl_2$, 2 U RiboLock Ribonuclease inhibitor (Life technologies), 1 μl PicoGreen Quantitation Reagent (Life technologies). Before starting the reaction, 1 μM final concentration of the protein was added to the mixture together with the inhibitor (from 0 to 50 μM). The reactions were followed for 1 h at 30 °C on a TECAN Infinite 200 PRO microplate reader, measuring the growth of PicoGreen fluorescence (Ex/Em = 485/530 nm) due to the formation of dsRNA. The final fluorescence values were calculated as the average of four independent experiments. Measurements of activity (*i.e.* linear slope of fluorescence increase in time) *vs.* inhibitor concentration were used to estimate the IC50 values of the two *in silico* selected compounds using the program GraFit5 (Erithacus software), and the equation $Y=(Range/(1+(X/IC50)^S)$, where *Range* is the value observed for the uninhibited RdRp, and *s* is a slope factor.

### 2.5. DENV3 and WNV RdRp/HeE1-2Tyr inhibition kinetic assay

Enzyme kinetics experiments were performed in order to gain insight on the inhibition mechanism of **HeE1-2Tyr** relative to either the poly(C) RNA template or the GTP substrate. Briefly, we performed standard enzymatic reactions on both DENV3 and WNV RdRps in the presence of increasing amounts of the inhibitor (from 0 to 4 μM) where: *i.* the poly(C) concentration was varied (from 78 ng to 10 μg, in 200 μl final volume) at constant GTP concentration (100 μM); or *ii.* the GTP concentration was varied (from 0 to 1 mM), at 10 μg poly(C) constant concentration in 200 μl reaction volume. The assays were performed using a TECAN Infinite 200 PRO microplate reader; the results were analyzed through Lineweaver–Burk plots (1/V versus 1/[S]) at varying **HeE1-2Tyr** concentrations.

### 2.6. In cell inhibition assays

#### 2.6.1. Strain information

DENV-1 Djibouti (strain D1/H/IMTSSA/98/606), PMID:11369871; DENV-2 Martinique (strain H/IMTSSA-MART/98-703), PMID:11027645; DENV-3 Bolivia (strain 4025), PMID:19505253; DENV-4 Dakar (strain HD34460, WRCEVA); WNV Uganda 956 D117, WRCEVA; YFV Bolivia 88-99; YFV Sudan M 90-5 TVP 3230, WRCEVA, YFV Uganda MR896 TVP 3236, WRCEVA; YFV Nigeria A-Adeoye TVP 3223, WRCEVA. Sequence of primers and probe are available on request.

#### 2.6.2. Antiviral assay

The amount of each virus in the assay was calibrated such that the replication growth was not yet plateaued at readout time, depending on the virus species (day 4 for most DENVs, and day 3 for WNV and YFV). Approximate MOI (Multiplicity Of Infection) varies from 0.2 to 0.01 depending on the virus strain. One day prior to infection, $5 \times 10^4$ Vero E6 cells (or $10^5$ HEK 293 cells for YFV assay) were seeded in 100 μl of medium (with 2.5% FCS) in each well of 96-well cell culture plates. The next day, 8 serial two-fold dilutions of the compound (from 20 μM to 0.16 μM), in duplicates or triplicates, were added to the cells (25 μl/well, in 2.5% FCS containing medium). Four Virus Control (VC) wells (per virus) were supplemented with 25 μl of medium. Fifteen minutes later, 25 μl per well of medium (2.5% FCS), containing the appropriate amount of diluted viral stock, were added to the 96-well plates.

Cells were cultivated for 3 or 4 days, after which 100 μl of the supernatant were collected for viral RNA purification. The infected supernatants were transferred to 96 wells S-Bloc from QIAgen, preloaded with VXL lysis buffer mix and extracted by the Cador Pathogen 96 QIAcube HT kit ran on QIAcube HT automat according to the manufacturer protocol. Purified RNAs were eluted in 80 μl. Viral RNAs were then quantified by real time RT-PCR (ABI 7900 HT Fast Real-Time PCR System) to determine viral RNA yield (SuperScript III Platinium one-step RT-PCR with Rox from Invitrogen or GoTaq Probe 1-step RT-PCR system from Promega), using 7.5 μl of RNA and 12.5 μl of RT-PCR mix using standard cycling parameters. Four 2-log dilutions of an appropriate T7-generated RNA containing known quantities of RNA (100 copies to 100 millions copies) were used to calibrate the quantification of each strain and serotype. Mean inhibition of virus yield in the triplicates or duplicates were plotted using Kaleidagraph software (Synergy Software) and the best sigmoidal curve was determined by a macro in this software: (Inhibition, Y is given by $Y = 100/(m0/m1)^{m2}$). This macro allowed us to determine the IC50, half maximal inhibitory concentration.

#### 2.6.3. Cytotoxicity assay

One day prior to the assay $5 \times 10^4$ Vero E6 cells (or $10^5$ HEK 293 cells) were seeded in 100 μl of medium (with 2.5% FCS) in each well of a 96-well titer plates. The next day, two-fold serial dilutions of the compounds (from 200 μM to 6.2 μM), in duplicates or triplicates, were added to the cells (25 μl/well, in 2.5% FCS). Six cell control (CC) wells were supplemented with 25 μl medium containing two-fold serial dilution of an equivalent amount of DMSO. Eight wells were not seeded with cells and served as background control of fluorescence for the plates. Cells were cultivated for 3 (HEK 293) or 4 (Vero E6) days, after which the supernatant was removed and replaced with 70 μl of medium containing CellTiter-Blue reagent (Promega) and further incubated for 90 min at 37 °C. Fluorescence of the plates was then read on a TECAN Infinite M 200 Pro reader. The cell viabilities in percent were calculated as 100 x (mean value of X- Background without cells)/(CC − background).

### 2.7. Crystal structure of the DENV3 RdRp in complex with HeE1-2Tyr

Sitting drop crystallization experiments on DENV3 RdRp (9 mg/ml) were assembled by means of an Oryx-8 crystallization robot (Douglas Instruments, East Garston, UK), using 0.3 μl droplets containing 50/50% of the protein/precipitant solutions, following the protocol already described (Noble et al., 2013). Crystals were obtained after 1 week at 20 °C, in 20–50 mM $MgCl_2$, 100 mM HEPES pH 7.5, and 22% w/v Poly(acrylic acid sodium salt). Before X-ray data collection, crystals were soaked for 48 h in a cryoprotectant solution (25–55 mM $MgCl_2$, 100 mM HEPES pH 7.5, 22% w/v Poly(acrylic acid sodium salt), and 25% glycerol) containing 10 mM **HeE1-2Tyr** in the presence of 10 μg of Poly-C and 100 μM GTP, and then flash-cooled in liquid nitrogen. The DENV3 RdRp/**HeE1-2Tyr** crystals diffracted to a maximum resolution of 3.0 Å using synchrotron radiation on beam-line BM30 at the European Synchrotron Radiation Facility (ESRF-Grenoble, France). X-ray diffraction data were indexed and scaled using XDS (Kabsch, 2010) (Table 1).

The three-dimensional structure of DENV-RdRp/**HeE1-2Tyr** was solved by the Molecular Replacement method using the program

MOLREP (Vagin and Teplyakov, 1997) and a search model based on the DENV3 RdRp 3D structure (PDB-id **4HHJ**; (Noble et al., 2013)). The single RdRp molecule present in the crystal asymmetric unit was subjected to rigid-body refinement, and subsequently constrained refined using REFMAC5 (Steiner et al., 2003). A random set comprising 5% of the data was omitted from refinement for R-free calculation. After a few refinement cycles of the free RdRp structure, additional electron density was clearly visible in the Fo-Fc map (Fig. 3, left inserts), allowing to fit the **HeE1-2Tyr** molecule in a location between the priming loop and the fingers domain. Manual rebuilding with COOT (Emsley et al., 2010), and additional refinement with BUSTER (Smart et al., 2012) and REFMAC5 were subsequently performed. Data collection, refinement statistics as well as stereochemical quality of the model are summarized in Table 1. Atomic coordinates and structure factors for DENV3 RdRp in complex with **HeE1-2Tyr** have been deposited in the PDB (Berman et al., 2000), with accession code **5IQ6**.

### 2.8. DENV3 RdRp mutants production

DENV3 RdRp mutants were generated from the pET15b-DENV3 clone using a QuikChange site-directed mutagenesis kit (Stratagene). According to the manufacturer's instructions primers used for mutagenesis are reported in Supplementary material. DENV3 RdRp mutants were expressed in *E. coli* BL21pLys cells and purified as reported for the wt protein.

### 2.9. DENV3 RdRp wt and mutants/HeE1-2Tyr binding assays

*In vitro* inhibitor binding assays were performed at 30 °C in a Varian Cary Eclipse Fluorescence Spectrophotometer, recording Trp fluorescence spectra between 300 and 400 nm (excitation 280 nm). 10 μl of **HeE1-2Tyr** (diluted in DMSO from 0 to 50 μM) were added to 170 μl of protein solution (final protein concentration 0.2 μM). The assay was performed for the wt protein also in the presence of ssRNA (final concentration 0.5 μM). Before the assay we verified that HeE1-2Tyr did not absorb/emit in the spectral range selected for our binding experiments. The values of fluorescence *vs*. inhibitor concentration were fitted with GraFit 5 (http://www.erithacus.com/grafit/) using the three parameter ($M$, $m$, $K_d$) equation:

$$F = M - \frac{(M-m)}{[P_T]}\,[PI] \text{ with } [PI] = \frac{[P_T]+[I_T]+K_d - \sqrt{([P_T]+[I_T]+K_d)^2 - 4[P_T][I_T]^2}}{2}.$$

Where $F$ is the fluorescence intensity, $[P_T]/[I_T]$ are the total protein/inhibitor concentrations, $M/m$ is the max/min of fluorescence, and $[PI]$ is the concentration of the protein bound to the inhibitor.

**Table 1**
X-ray data-collection and refinement statistics.

| | |
|---|---|
| **Data collection** | |
| Beam line & wavelength (Å) | ESRF BM30; 0.9798 |
| Space group | $C222_1$ |
| Unit-cell parameters (Å) | a = 162.0; b = 180.9; c = 58.1 |
| Molecules in a.u. | 1 |
| Resolution (Å) | 45.5–3.0 |
| Mosaicity (°) | 0.2 |
| Unique reflections | 17,202 (1279)[a] |
| Completeness (%) | 97.8 (99.4) |
| Redundancy | 4.0 (4.1) |
| Rmeas[b] (%) | 18.1 (96.5) |
| CC(1/2) (%) | 98.9 (59.5) |
| Average $I/\sigma$ ($I$) | 9.7 (1.8) |
| **Final model** | |
| R factor[c]/Rfree[d] (%) | 19.2/26.0 |
| r.m.s. bonds (Å) | 0.004 |
| r.m.s. angles (°) | 0.84 |
| Average protein *B* fac. | 65.5 |
| Average ligand *B* fac. (Å$^2$) | 118.8[e] |
| Residues in most favored regions (%) | 97% |
| Residues in additionally allowed regions (%) | 3% |
| LLDF[f] | 1.48 |
| ligand RSR[g] (%) | 26.0 |
| PDB-ID | **5IQ6** |

Values in parentheses are for the highest resolution shell.
[a] (3.08–3.0).
[b] $R_{meas} = (\Sigma\,(n/(n-1)\,\Sigma\,|I - (I)|)/\Sigma\, I \times 100$, where $I$ is intensity of a reflection and $(I)$ is its average intensity.
[c] $R_{factor} = \Sigma\,|F_o - F_c|/\Sigma\,|F_o| \times 100$.
[d] $R_{free}$ is calculated on 5% randomly selected reflections, for cross-validation.
[e] Ligand occupancy 1.
[f] Local Ligand Density Fit.
[g] Real Space R-value.

## 3. Results

### 3.1. Synthesis of HeE1-2Tyr

**HeE1-2Tyr** was obtained (Fig. 1) revisiting a synthetic route recently published for the preparation of functionalized pyridobenzothiazoles (Manfroni et al., 2012). According to this procedure, 2-methylbenzothiazole derivative **1** underwent two consecutive steps of demolition and reconstruction to produce the corresponding ethyl 1,3-benzothiazolacetate **2** in low yield and with poor reproducibility. In order to by-pass the limiting steps of the original method (Manfroni et al., 2012), compound **1** was directly functionalized at the C-2 methyl group by reaction with diethyl carbonate using NaH as a base to yield the acetate derivative **2** in 70% yield. Compound **2** was then reacted with Vilsmeier reagent to afford the acrylate derivate **3** which was used to build the pyridobenzothiazole nucleus of compound **4**, employing phenyl acetic anhydride (Morrill et al., 2014) in neat condition. Ester **4** was hydrolyzed under basic conditions to the corresponding acid **5**, which was coupled with Tyr methyl ester hydrochloride, using TBTU reagent, to give amide **6** that was then hydrolyzed into target compound **HeE1-2Tyr** under mild conditions with LiOH. To evaluate the enantiomeric purity of **HeE1-2Tyr**, its D enantiomer **8** was also synthesized (see Supplementary material for the compound preparation). Chiral HPLC analysis using the **HeE1-2Tyr** alone and in mixture with its D enantiomer **8** highlighted 100% of enantiomeric excess for both compounds meaning that no racemization occurred during mild hydrolysis conditions (Fig. S1).

### 3.2. In silico docking search

A virtual screening procedure was applied to select new potential inhibitors of DENV3 RdRp. We performed an *in silico* docking search exploring a wide region around the DENV3 RdRp active site (pdb-id: **2J7U** (Yap et al., 2007)), using a proprietary library of compounds originally focused on HCV RdRp inhibition (Manfroni et al., 2014a,b; Barreca et al., 2013; Manfroni et al., 2012). The docking search produced a list of compounds with predicted binding free energy values ranging between −5.65 kcal/mol and −10.05 kcal/mol. The top 2 compounds i.e. **HeE1-2SO$_2$** (compound **3c** in (Manfroni et al., 2012)) and **HeE1-2Tyr**, characterized by the lowest docking energy (−10.05 kcal/mol and −9.52 kcal/mol respectively; Fig. S3) were selected for *in vitro* analysis of RdRp inhibitory activity.

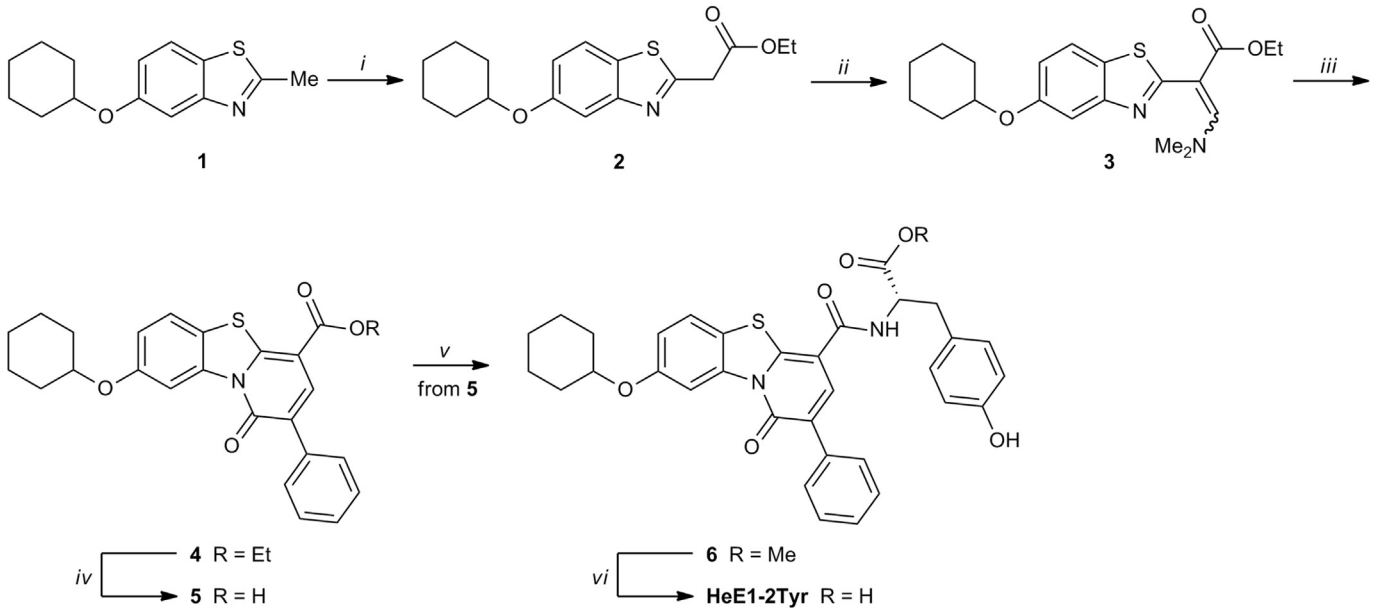


**Fig. 1. Synthetic pathway employed for the preparation of HeE1-2Tyr**. Reagents and conditions: *i*) diethyl carbonate, 60% NaH, dry THF, reflux; *ii*) Vilsmeier reagent, 90 °C; *iii*) phenylacetic anhydride, 110 °C, neat; *iv*) aq. 10% NaOH/MeOH (1:5), 75 °C. *v)* Tyr methyl ester HCl, TBTU, DIPEA, DMSO, rt; *vi)* aq 1N LiOH, 1,4-dioxane, rt.

### 3.3. *In vitro inhibition of DENV3 and WNV RdRp*

Both **HeE1-2Tyr** and **HeE1-2SO2** (Manfroni et al., 2012) showed inhibitory activity against DENV3 and WNV RdRps in the μM range. Since our *in vitro* inhibition assay is based on ssRNA template (Poly-C) we could not discriminate between initiation and elongation phases of RNA polymerization. In particular, **HeE1-2SO2** inhibited DENV3 and WNV RdRps with $IC_{50} = 2.8 \pm 0.5$ μM and $2.5 \pm 1.3$ μM, respectively, whereas **HeE1-2Tyr** $IC_{50}$ values against DENV3 and WNV RdRps were $1.5 \pm 0.2$ μM and $3.4 \pm 0.4$ μM, respectively (Fig. 2A).

Since only **HeE1-2Tyr** showed inhibition activity in cell-based assays (see below) we further characterized this compound analyzing the RdRp kinetic properties in the presence of the inhibitor. The Lineweaver–Burk plots for both DENV3 (Fig. 2 B,C) and WNV RdRp (not shown) highlighted a non-competitive inhibition mechanism relative to both the poly(C) and the GTP substrates.

### 3.4. *In cell inhibition assays*

**HeE1-2Tyr** and **HeE1-2SO$_2$**, were tested for antiviral activity in cell assays (HEK 293 and Vero E6 cells). **HeE1-2SO$_2$** did not show any activity whereas **HeE1-2Tyr** was able to inhibit an Ugandan strain of WNV with an $IC_{50} = 2.1 \pm 0.7$ μM, as well as all the four DENV serotypes, with $IC_{50}$ ranging from 6.8 to 15 μM (Table 2). The cytotoxicity of **HeE1-2Tyr** versus Vero E6 cells was ~115 ± 35 μM, allowing a reasonably good selectivity index for a starting hit compound. Additionally, upon infection of human HEK 293 cells ($CC_{50} = 50$ μM), **HeE1-2Tyr** was found to inhibit clinical strains of YFV with $IC_{50}$ values ranging from 3.9 to 12 μM (Table 2).

### 3.5. *DENV3 RdRp/HeE1-2Tyr crystal structure*

The crystal structure of DENV3 RdRp/**HeE1-2Tyr** complex was obtained after soaking the protein crystals with the inhibitor (10 mM) in the presence of 10 μg of Poly-C and 100 μM of GTP, for 48 h. Poly-C and GTP were added to promote diffusion and binding of the inhibitor as observed in our previous works on Norovirus RdRp (Tarantino et al., 2014; Croci et al., 2014a; Croci et al., 2014b). After the molecular replacement solution and a few refinement cycles, additional electron density in the Fo-Fc map (Fig. 3, left inserts) allowed to fit the **HeE1-2Tyr** molecule between the priming loop and the fingers domain (binding Site 1; Fig. 3), at about 10 Å from the *in silico* docking site (Fig. S3). Several other crystals, soaked with 10 mM **HeE1-2Tyr** in the absence of Poly-C and GTP, exhibited a similar Fo-Fc map peak in the same zone, thus excluding a mistaken interpretation of the electron density (*e.g.* inhibitor for nucleotides). Interestingly, **HeE1-2Tyr**, which is a bulky molecule with a high degree of conformational freedom, is folded on itself in a rather compact conformation with its phenolic ring in stacking interaction with the pyridobenzothiazole moiety. Such closed shape is reminiscent of the stacking interaction of two RNA bases, and is stabilized by additional stacking with the side chain of Trp795 in the priming loop (Fig. 3). The structural parallelism between the shape of **HeE1-2Tyr** and a small RNA fragment is further reinforced by the presence of the negatively charged carboxylate group of the inhibitor that mimics the nucleotide backbone phosphate. **HeE1-2Tyr** induces only a slight perturbation of the protein structure (Cα r.m.s.d. of 0.43 Å relative to pdb **4HHJ**). In particular we observed flipping of Val603 ψ main chain dihedral angle by 180°, due to steric hindrance of the inhibitor cyclohexane moiety; this caused the loss of a H-bond with the Asn492 side chain, that moves away through ~100° side chain rotation. The inhibitor cyclohexane ring is hosted in a shallow depression of the protein surface in close contact with the amino acids 603-606 and with the side chain of Asn492.

The **HeE1-2Tyr** binding site (Site 1) matches the site already observed for the DENV RdRp inhibitor NITD107 (pdb-id **3VWS** (Noble et al., 2013)), where, in place of the two stacking rings of **HeE1-2Tyr**, two inhibitor molecules (arranged in antiparallel stacking interaction) are present. Very recently, the crystal structures of a new class of potent DENV RdRp non-nucleoside inhibitors have been published (Noble et al., 2016; Yokokawa et al., 2016), showing that the compounds bind in a cavity formed by the priming loop and the thumb domain. Such cavity and the **HeE1-2Tyr** Site 1 are separated by the tip of the priming loop (amino acids

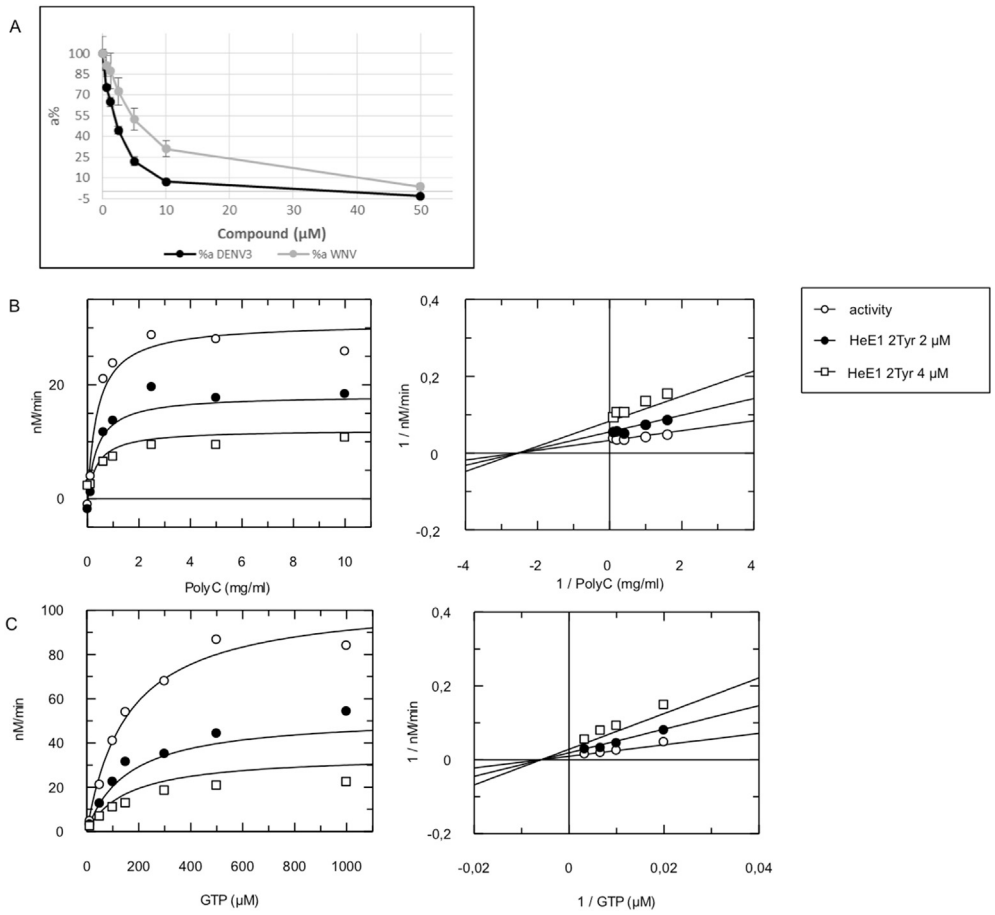


**Fig. 2. HeE1-2Tyr RdRp inhibition. A** The inhibitory effect of **HeE1-2Tyr** on DENV3 and WNV RdRp activity was measured by the decrease in relative fluorescence growth rate (a% corresponds to the fluorescence growth rate expressed in percentage of the growth rate without the inhibitor). An average result of four independent experiments is shown, with error bars indicating standard deviations. **B** Lineweaver-Burk double reciprocal plot showing the **HeE1-2Tyr** non-competitive inhibition mechanism on DENV3 RdRp, relative to the PolyC template, with a Ki values of 0.64 ± 0.09 μM. **C** Lineweaver-Burk double reciprocal plot showing the **HeE1-2Tyr** non-competitive inhibition mechanism on DENV3 RdRp, relative to the GTP substrate, with Ki values of 1.96 ± 0.20 μM. **B** and **C** are the average results of four independent experiments.

794-796), being about 14 Å apart.

Overall, **HeE1-2Tyr** appears to mimic the possible initial interaction between template RNA and the enzyme during the first steps of RNA polymerization. Therefore, the crystal structure would suggest that the inhibitor may interfere with the incoming RNA template, in principle hinting at a competitive inhibition mechanism *vs*. the RNA substrate (Fig. 3). To validate such hypothesis we performed a Trp fluorescent binding assay, in the absence/presence of ssRNA. The $K_d$ values obtained were not affected by the presence of the substrate ($K_d = 5.5 \pm 0.3$ μM and $5.8 \pm 0.6$ μM in the absence/presence of ssRNA, respectively).

### 3.6. DENV3 RdRp Trp795Ala and Asn492Phe mutants

To further characterize the protein-inhibitor interactions we produced two point mutants, Asn492Phe and Trp795Ala, to modify residues of the inhibitor binding site. The binding affinity of **HeE1-2Tyr** for the Asn492Phe RdRp mutant was unaffected (DENV3 wt RdRp $K_d = 5.5 \pm 0.3$ μM *vs* Asn492Phe $K_d = 4.5 \pm 0.8$ μM, Fig. 4). On the contrary, **HeE1-2Tyr** dissociation constant for the Trp795Ala mutant increased by a factor of 2, to $10.5 \pm 0.5$ μM (Fig. 4). As a result, the polymerase activity of both mutants was inhibited by **HeE1-2Tyr** to the same extent observed for the wt RdRp (the polymerase activity of the protein was unaltered by the two mutations).

The experimental results described above outline a conceptual discrepancy between the crystallographic data (suggesting a competitive inhibition mechanism), the inhibition kinetics (consistent with a non-competitive inhibition mechanism) and the two RdRp mutants that, despite the designed perturbation of the ligand binding site, are inhibited by **HeE1-2Tyr** to the same extent of the wt enzyme.

### 3.7. DENV3 RdRp Cys753Glu and Arg749Ala mutants

In order to address the above mentioned discrepancy, we speculated that during the enzyme catalytic cycle the RdRp priming loop must move out of the active site to make room for the crescent dsRNA. The priming loop relocation during RNA elongation might thus expose a previously buried portion of the thumb domain where **HeE1-2Tyr** may bind as a non-competitive inhibitor.

To test such hypothesis we deleted *in silico* the RdRp priming loop, i.e. amino acids comprised between His786 and Asp808 (leaving an open gap in the polypeptide chain), exposing a new region of the thumb subdomain (we refer to such modified RdRp model as RdRp*). The newly exposed region was then explored *in silico*, searching for alternative **HeE1-2Tyr** docking site(s). The docking procedure allowed to identify a new potential binding site for **HeE1-2Tyr** (Site 2; Fig. 5; binding $\Delta G = -8.69$ kcal/mol; predicted $Ki = 0.43$ μM) located at the N-terminal end of the 750-776

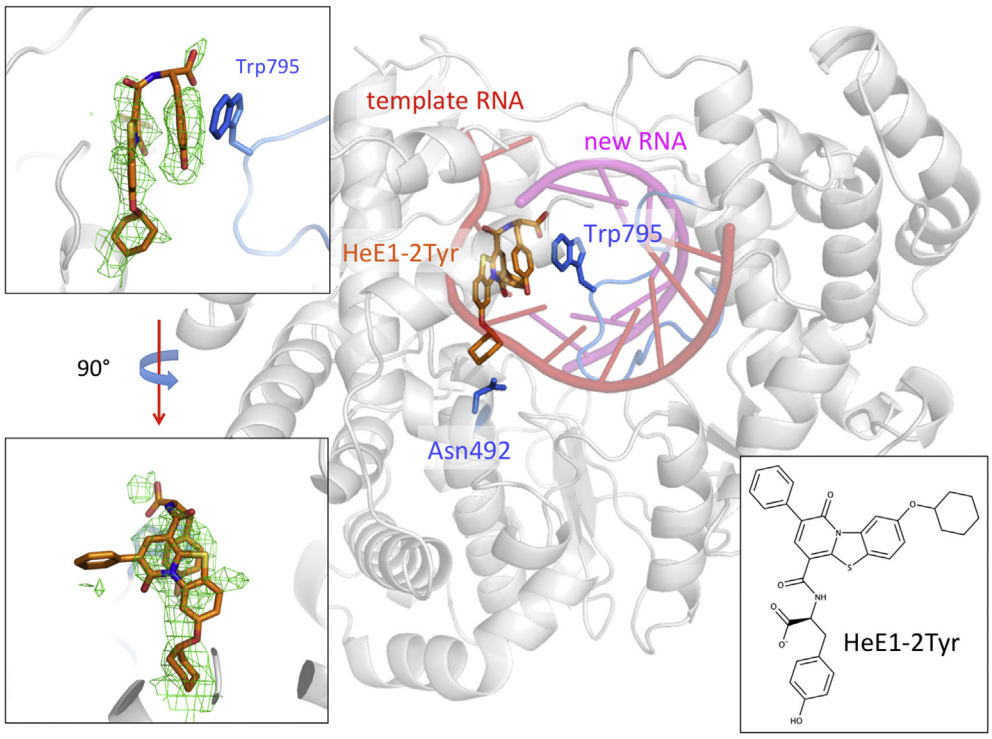


**Fig. 3. Crystal structure of DENV3 RdRp in complex with HeE1-2Tyr. HeE1-2Tyr** (sticks with orange carbon atoms) bound to RdRp (gray cartoon): the priming loop is shown as blue cartoon, Trp795 and Asn492 interacting with the inhibitor, are shown as blue sticks. Template and newly formed RNA have been superimposed on the crystal structure as red and pink cartoons, respectively, to illustrate possible inhibitor interference with protein activity (modeled from the structure of Norwalk Virus polymerase, pdb-id **3BSO**). **Left inserts**: the Fo-Fc electron density map contoured at 2.5 sigma calculated after the initial refinement cycles without the inhibitor (shown for reference). Picture drawn with Pymol (www.pymol.org). **Lower right insert: HeE1-2Tyr** chemical structure. (For interpretation of the references to colour in this figure legend, the reader is referred to the web version of this article.)

**Table 2**
Cell-based inhibitions and cytotoxicity of HeE1-2Tyr and reference compound NITD 008.

| | HeE1-2Tyr | NITD 008 |
|---|---|---|
| | CC50 | |
| Vero E6 | 115 ± 35[a] | >100 |
| | IC50 | |
| DENV-1 Djibouti | 6.8 | 0.39 |
| DENV-2 Martinique | 15 ± 5 | 0.82 |
| DENV-3 Bolivia | 10 ± 0.6[a] | 0.8 |
| DENV-4 Dakar | 7.7 ± 2.2[a] | ND |
| WNV Uganda | 2,1 ± 0,7[a] | 0.85 |
| | CC50 | |
| HEK-293 | 50 ± 10[a] | ND |
| | IC50 | |
| YFV Bolivia | 3.9 ± 1.4[a] | 0.35 ± 0.1[a] |
| YFV Uganda | 8.3 | ND |
| YFV Nigeria | 12 | ND |
| YFV Sudan | 3.1 | 0.27 |

Dengue viruses and WNV were assayed in Vero E6 cells. YFV strains were assayed in HEK 293 cells. Individual CC50 and IC50 values (in μM) are the mean of triplicates. [a] indicates mean and variance of two or three independent experiments.

α-helix (at ~18 Å distance from Site 1). **HeE1-2Tyr** would adopt an extended conformation in Site 2, stabilized by several interactions with the protein, such as H-bonds to Cys753, to the main chain of Pro784, and a salt bridge to Arg749 (Fig. 5).

In order to validate the results of such computational model we produced two point mutations on wt RdRp (Cys753Glu and Arg749Ala; Fig. 5), predicted to perturb the **HeE1-2Tyr** binding to Site 2. Since Site 2 is not accessible when the protein is not involved in the catalytic cycle, the affinity of the protein for **HeE1-2Tyr** is not affected by the two point mutations ($K_d$ = 5.2 ± 0.3 μM and 5.7 ± 0.5 μM for Cys753Glu and Arg749Ala, respectively). In the presence of the Cys753Glu mutation, RdRp proved slightly less susceptible to **HeE1-2Tyr** inhibition (IC50 raised from 1.5 ± 0.2 μM (wt) to 5.0 ± 0.8 μM (Fig. 6). Moreover, even if the Arg749Ala mutation produced a considerable decrease in protein activity (~80% drop), suggesting an involvement of Arg749 in RNA binding, the residual protein activity was unaffected by **HeE1-2Tyr** up to an inhibitor concentration of 50 μM (Fig. 6), in keeping with the mutation design aims. Thus, the mutational results suggest that the Site 2 region is relevant for RdRp inhibition by **HeE1-2Tyr**.

## 4. Discussion

**HeE1-2Tyr** is firstly presented here as a new inhibitor of DENV3 RdRp endowed with significant inhibitory activity against DENV and other flaviviruses (i.e. WNV, YFV) in cell cultures. Nevertheless, the biochemical and structural analyses presented entail a series of conflicting results. In particular, we observed an evident discrepancy between the crystal structure, which would suggest that **HeE1-2 Tyr** at Site 1 competes with RNA binding, and the non-competitive inhibition mechanism highlighted by the kinetics data. Such discrepancy was further stressed by the observation that a selected point mutation expected to perturb the inhibitor binding site (Trp795Ala in the priming loop) did not decrease **HeE1-2Tyr** inhibitory activity *in vitro*, suggesting that the inhibition site might be different from the binding site observed in the crystal structure. In order to address such incongruity we speculated that, when the enzyme is bound to the crescent dsRNA, the inhibitor cannot bind to the priming loop with the same modality observed in the crystal

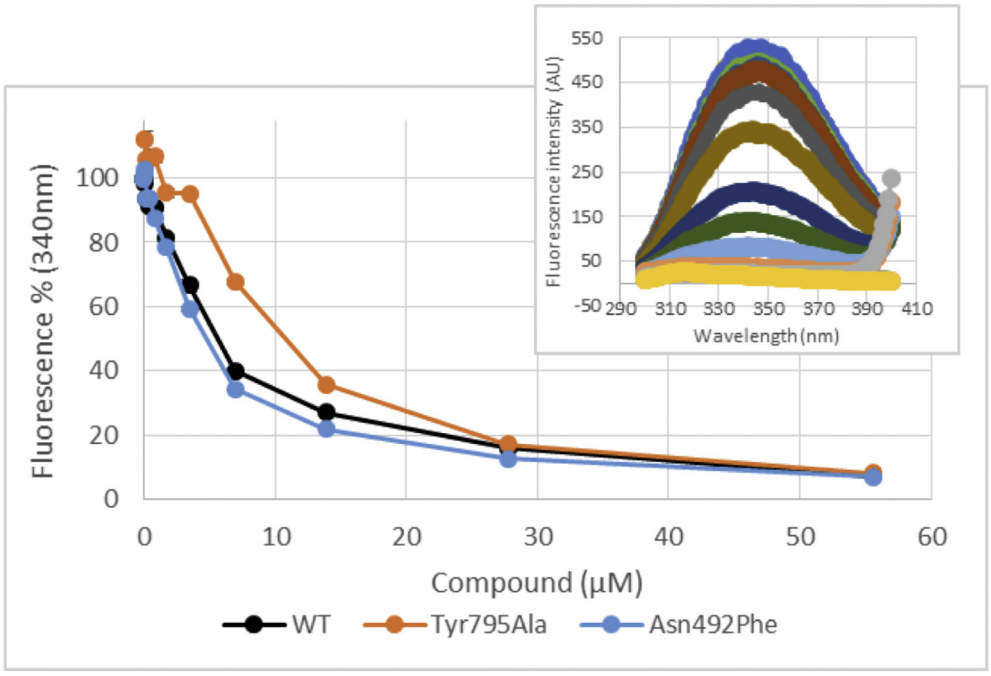


**Fig. 4. Binding of DENV3 RdRp to HeE1-2Tyr**. The binding of the **HeE1-2Tyr** to RdRp wt, Asn492Phe mutant and Trp795Ala mutant was monitored following the variation of protein Trp fluorescence (with a peak around 340 nm). **The insert panel** shows the experimental curves collected for the wt protein.

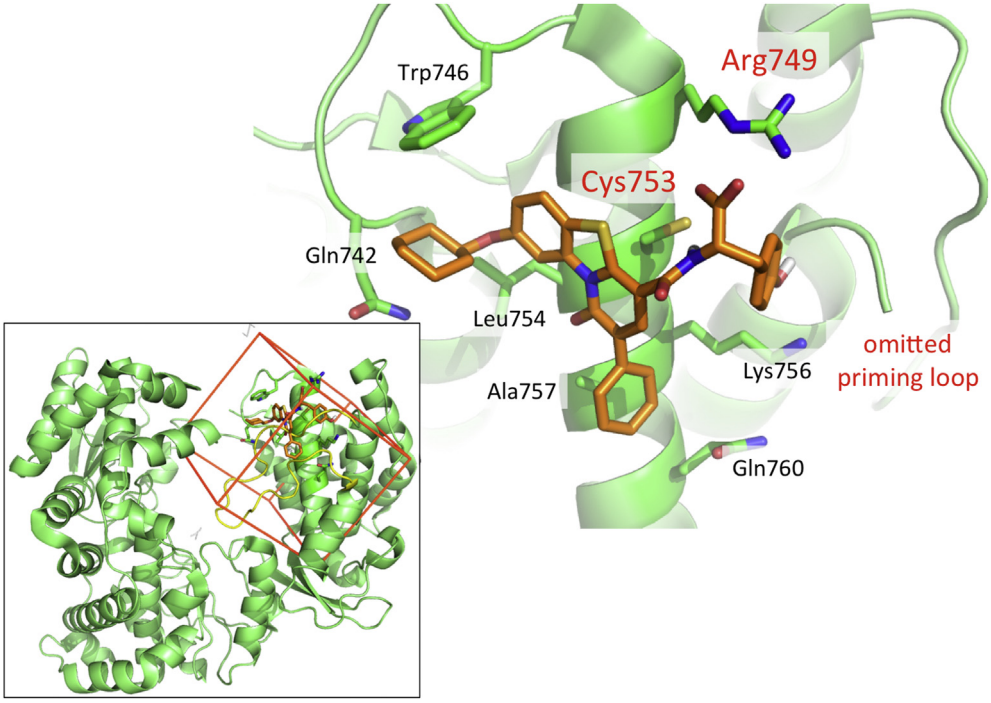


**Fig. 5.** ***in silico*** **docking of HeE1-2Tyr on RdRp without the priming loop. HeE1-2Tyr** (sticks with orange carbon atoms) docked on the thumb domain of RdRp (green cartoons), interacting with Arg749, Cys753 and other amino acids (shown as sticks with green carbon atoms) after the deletion of the priming loop. **The lower insert** shows the overall protein structure with the omitted priming loop (yellow cartoon) and the extent of the region explored with the new *in silico* docking search. (For interpretation of the references to colour in this figure legend, the reader is referred to the web version of this article.)

structure. In fact, it is known that RdRp must undergo a significant conformational change during transition from the initiation to the elongation complex. The priming loop, after its initial role in assisting replication of the first nucleotides, must move out of the RdRp active site to allow the accommodation of the growing dsRNA (Choi and Rossmann, 2009; Selisko et al., 2012) (modeled in Fig. 3). Hence, we speculated that relocation of the priming loop during RNA elongation might expose a previously buried portion of the thumb domain where **HeE1-2Tyr** might bind to exert its function as a non-competitive inhibitor. To verify such hypothesis we

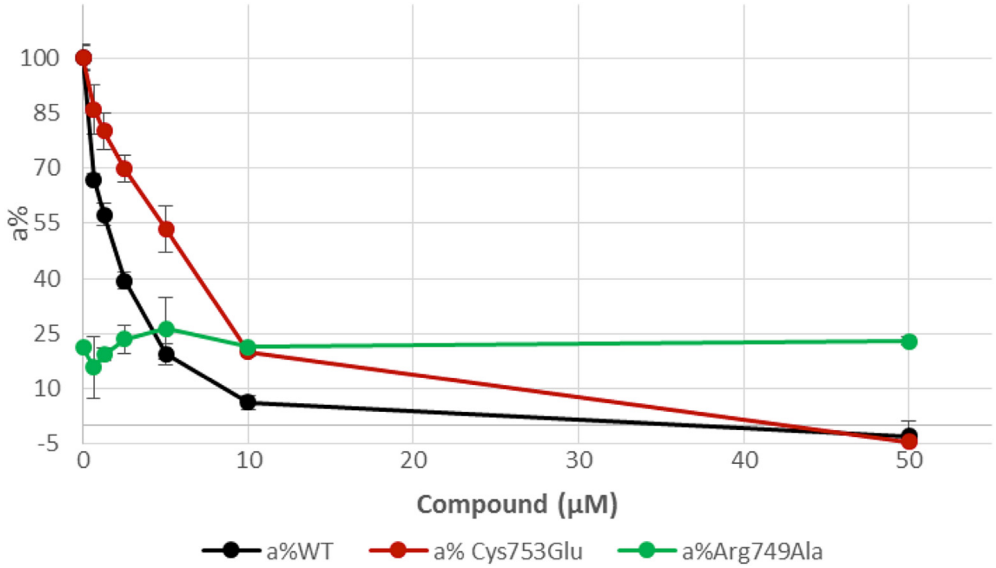


**Fig. 6. Inhibition of Cys753Glu and Arg749Ala mutants**. The inhibitory activity of **HeE1-2Tyr** on RdRp of DENV3 wt (black curve), Cys753Glu (red curve) and Arg749Ala (green curve) mutants was measured by the decrease in relative fluorescent slope (a% is the fluorescence over time slope expressed in percentage of the same slope in the absence of the inhibitor). An average result of four independent experiments is shown, with errors bars indicating standard deviations. (For interpretation of the references to colour in this figure legend, the reader is referred to the web version of this article.)

performed a specific *in silico* docking search on the thumb domain of RdRp* (priming loop deleted), to mimic the protein state achieved during RNA elongation. Such procedure allowed us to propose Site 2 as a new possible binding site for **HeE1-2Tyr**. We demonstrated that the mutation of either Cys753Glu or Arg749Ala expected to perturb inhibitor binding, caused a drop of **HeE1-2Tyr** inhibitory potency.

It is known that hepatitis C virus RdRp activity is affected by non-nucleoside allosteric inhibitors that bind four different sites distal to the enzyme active site; two of these are located in the palm domain, and two in the thumb domain (Barreca et al., 2011; Haudecoeur et al., 2013). Notably, their mechanism of RdRp inhibition is not conclusively known; however it has been suggested that certain inhibitors act by preventing conformational changes that alter both the structure and internal protein dynamics crucial for RNA replication (Davis and Thorpe, 2013). Interestingly, the location of DENV3 RdRp Site 2 in the thumb domain is different from that of the thumb Site I and II in HCV polymerase (Haudecoeur et al., 2013). Site 2 resides along the exit pathway of the newly formed dsRNA (Fig. 3), therefore **HeE1-2Tyr** inhibition can be (at least partially) due to a hindering action on the polymerase translation along the RNA. Furthermore, Site 2 is distant from the NS5 methyltransferase-polymerase interface (Zhao et al., 2015) (mainly involving the fingers domain of RdRp), which is then unlikely to be affected by HeE1-2Tyr binding.

Despite the biochemical data collected so far, we cannot rule out that, besides RdRp, other flaviviral proteins might be affected by **HeE1-2Tyr**, also considering the inhibitor's potential structural similarity with a dinucleotide in stacking conformation. Nevertheless, the preliminary data of **HeE1-2Tyr** activity in infected cells are encouraging, and suggest that synergism with further molecular design and biophysical data can lead to a new class of potent and selective anti flaviviral compounds.

## Funding information

This work has been founded by European Commission SILVER project, within the 7th Framework Program Cooperation Project Grant Agreement No. 2606444 and by Italian government project SIR Grant number: RBSI14C78S.

## Acknowledgements

We thank the beam line scientists from the ESRF facility for support during data collections.

We thank Dr. Roccaldo Sardella for chiral HPLC analysis on **HeE1-2Tyr** and compound 8 and Dr. Pilar Franco from Chiral Tecnologies-Daicel Europe (Illkirch, France) who generously provided us the CHIRALPAK® ZWIX(+) and CHIRALPAK® ZWIX(-) columns.

We thank Prof. Julien Lescar who generously provided us with the DENV3 RdRp plasmid.

We thank Dr. Riccardo Borgonovo who partly contributed to the reported studies during his graduation internship.

## Appendix A. Supplementary data

Supplementary data related to this article can be found at http://dx.doi.org/10.1016/j.antiviral.2016.09.007.

## References

Barreca, M.L., Iraci, N., Manfroni, G., Cecchetti, V., 2011. Allosteric inhibition of the hepatitis C virus NS5B polymerase: in silico strategies for drug discovery and development. Future Med. Chem. 3, 1027–1055.

Barreca, M.L., Manfroni, G., Leyssen, P., Winquist, J., Kaushik-Basu, N., Paeshuyse, J., Krishnan, R., Iraci, N., Sabatini, S., Tabarrini, O., Basu, A., Danielson, U.H., Neyts, J., Cecchetti, V., 2013. Structure-based discovery of pyrazolobenzothiazine derivatives as inhibitors of hepatitis C virus replication. J. Med. Chem. 56, 2270–2282.

Berman, H.M., Westbrook, J., Feng, Z., Gilliland, G., Bhat, T.N., Weissig, H., Shindyalov, I.N., Bourne, P.E., 2000. The protein data bank. Nucleic Acids Res. 28, 235–242.

Choi, K.H., Rossmann, M.G., 2009. RNA-dependent RNA polymerases from Flaviviridae. Curr. Opin. Struct. Biol. 19, 746–751.

Croci, R., Pezzullo, M., Tarantino, D., Milani, M., Tsay, S.C., Sureshbabu, R., Tsai, Y.J., Mastrangelo, E., Rohayem, J., Bolognesi, M., Hwu, J.R., 2014a. Structural bases of norovirus RNA dependent RNA polymerase inhibition by novel suramin-related compounds. PLoS One 9, e91765.

Croci, R., Tarantino, D., Milani, M., Pezzullo, M., Rohayem, J., Bolognesi, M., Mastrangelo, E., 2014b. PPNDS inhibits murine Norovirus RNA-dependent RNA-

polymerase mimicking two RNA stacking bases. FEBS Lett. 588, 1720–1725.
Daep, C.A., Munoz-Jordan, J.L., Eugenin, E.A., 2014. Flaviviruses, an expanding threat in public health: focus on dengue, West Nile, and Japanese encephalitis virus. J. neurovirology 20, 539–560.
Davis, B.C., Thorpe, I.F., 2013. Thumb inhibitor binding eliminates functionally important dynamics in the hepatitis C virus RNA polymerase. Proteins 81, 40–52.
Emsley, P., Lohkamp, B., Scott, W.G., Cowtan, K., 2010. Features and development of Coot. Acta Crystallogr. Sect. D. 66, 486–501.
Haudecoeur, R., Peuchmaur, M., Ahmed-Belkacem, A., Pawlotsky, J.M., Boumendjel, A., 2013. Structure-activity relationships in the development of allosteric hepatitis C virus RNA-dependent RNA polymerase inhibitors: ten years of research. Med. Res. Rev. 33, 934–984.
Kabsch, W., 2010. Xds. Acta Crystallogr. D. Biol. Crystallogr. 66, 125–132.
Leyssen, P., De Clercq, E., Neyts, J., 2000. Perspectives for the treatment of infections with Flaviviridae. Clin. Microbiol. Rev. 13, 67–82 table of contents.
Lim, S.P., Noble, C.G., Shi, P.Y., 2015. The dengue virus NS5 protein as a target for drug discovery. Antivir. Res. 119, 57–67.
Mackenzie, J.S., Gubler, D.J., Petersen, L.R., 2004. Emerging flaviviruses: the spread and resurgence of Japanese encephalitis, West Nile and dengue viruses. Nat. Med. 10, S98–S109.
Malinoski, F.J., Hasty, S.E., Ussery, M.A., Dalrymple, J.M., 1990. Prophylactic ribavirin treatment of dengue type 1 infection in rhesus monkeys. Antivir. Res. 13, 139–149.
Manfroni, G., Cannalire, R., Barreca, M.L., Kaushik-Basu, N., Leyssen, P., Winquist, J., Iraci, N., Manvar, D., Paeshuyse, J., Guhamazumder, R., Basu, A., Sabatini, S., Tabarrini, O., Danielson, U.H., Neyts, J., Cecchetti, V., 2014a. The versatile nature of the 6-aminoquinolone scaffold: identification of submicromolar hepatitis C virus NS5B inhibitors. J. Med. Chem. 57, 1952–1963.
Manfroni, G., Manvar, D., Barreca, M.L., Kaushik-Basu, N., Leyssen, P., Paeshuyse, J., Cannalire, R., Iraci, N., Basu, A., Chudaev, M., Zamperini, C., Dreassi, E., Sabatini, S., Tabarrini, O., Neyts, J., Cecchetti, V., 2014b. New pyrazolobenzothiazine derivatives as hepatitis C virus NS5B polymerase palm site I inhibitors. J. Med. Chem. 57, 3247–3262.
Manfroni, G., Meschini, F., Barreca, M.L., Leyssen, P., Samuele, A., Iraci, N., Sabatini, S., Massari, S., Maga, G., Neyts, J., Cecchetti, V., 2012. Pyridobenzothiazole derivatives as new chemotype targeting the HCV NS5B polymerase. Bioorg Med. Chem. 20, 866–876.
Morrill, L.C., Stark, D.G., Taylor, J.E., Smith, S.R., Squires, J.A., D'Hollander, A.C., Simal, C., Shapland, P., O'Riordan, T.J., Smith, A.D., 2014. Organocatalytic Michael addition-lactonisation of carboxylic acids using alpha,beta-unsaturated trichloromethyl ketones as alpha,beta-unsaturated ester equivalents. Org. Biomol. Chem. 12, 9016–9027.
Morris, G.M., Huey, R., Lindstrom, W., Sanner, M.F., Belew, R.K., Goodsell, D.S., Olson, A.J., 2009. AutoDock4 and AutoDockTools4: automated docking with selective receptor flexibility. J. Comput. Chem. 30, 2785–2791.
Noble, C.G., Lim, S.P., Arora, R., Yokokawa, F., Nilar, S., Seh, C.C., Wright, S.K., Benson, T.E., Smith, P.W., Shi, P.Y., 2016. A conserved pocket in the Dengue virus polymerase identified through fragment-based screening. J. Biol. Chem. 291, 8541–8548.
Noble, C.G., Lim, S.P., Chen, Y.L., Liew, C.W., Yap, L., Lescar, J., Shi, P.Y., 2013. Conformational flexibility of the Dengue virus RNA-dependent RNA polymerase revealed by a complex with an inhibitor. J. Virol. 87, 5291–5295.
O'Boyle, N.M., Banck, M., James, C.A., Morley, C., Vandermeersch, T., Hutchison, G.R., 2011. Open Babel: an open chemical toolbox. J. cheminformatics 3, 33.
Selisko, B., Potisopon, S., Agred, R., Priet, S., Varlet, I., Thillier, Y., Sallamand, C., Debart, F., Vasseur, J.J., Canard, B., 2012. Molecular basis for nucleotide conservation at the ends of the dengue virus genome. PLoS Pathog. 8, e1002912.
Smart, O.S., Womack, T.O., Flensburg, C., Keller, P., Paciorek, W., Sharff, A., Vonrhein, C., Bricogne, G., 2012. Exploiting structure similarity in refinement: automated NCS and target-structure restraints in BUSTER. Acta Crystallogr. Sect. D. 68, 368–380.
Steiner, R.A., Lebedev, A.A., Murshudov, G.N., 2003. Fisher's information in maximum-likelihood macromolecular crystallographic refinement. Acta Crystallogr. Sect. D. 59, 2114–2124.
Tarantino, D., Pezzullo, M., Mastrangelo, E., Croci, R., Rohayem, J., Robel, I., Bolognesi, M., Milani, M., 2014. Naphthalene-sulfonate inhibitors of human norovirus RNA-dependent RNA-polymerase. Antivir. Res. 102, 23–28.
Vagin, A., Teplyakov, A., 1997. MOLREP: an automated program for molecular replacement. J. Appl. Crystallogr. 30, 1022–1025.
Welsch, S., Miller, S., Romero-Brey, I., Merz, A., Bleck, C.K., Walther, P., Fuller, S.D., Antony, C., Krijnse-Locker, J., Bartenschlager, R., 2009. Composition and three-dimensional architecture of the dengue virus replication and assembly sites. Cell host microbe 5, 365–375.
Xu, H.T., Colby-Germinario, S.P., Hassounah, S., Quashie, P.K., Han, Y., Oliveira, M., Stranix, B.R., Wainberg, M.A., 2015. Identification of a pyridoxine-derived small-molecule inhibitor targeting Dengue virus RNA-dependent RNA polymerase. Antimicrob. Agents Chemother. 60, 600–608.
Yap, T.L., Xu, T., Chen, Y.L., Malet, H., Egloff, M.P., Canard, B., Vasudevan, S.G., Lescar, J., 2007. Crystal structure of the dengue virus RNA-dependent RNA polymerase catalytic domain at 1.85-angstrom resolution. J. Virol. 81, 4753–4765.
Yokokawa, F., Nilar, S., Noble, C.G., Lim, S.P., Rao, R., Tania, S., Wang, G., Lee, G., Hunziker, J., Karuna, R., Manjunatha, U., Shi, P.Y., Smith, P.W., 2016. Discovery of potent non-nucleoside inhibitors of Dengue viral RNA-dependent RNA polymerase from a fragment hit using structure-based drug design. J. Med. Chem. 59, 3935–3952.
Zhao, Y., Soh, T.S., Zheng, J., Chan, K.W., Phoo, W.W., Lee, C.C., Tay, M.Y., Swaminathan, K., Cornvik, T.C., Lim, S.P., Shi, P.Y., Lescar, J., Vasudevan, S.G., Luo, D., 2015. A crystal structure of the Dengue virus NS5 protein reveals a novel inter-domain interface essential for protein flexibility and virus replication. PLoS Pathog. 11, e1004682.